The Molecular and Electronic Structure of Octahedral Tris(phenolato)iron(III) Complexes and Their Phenoxyl Radical Analogues: A Mössbauer and Resonance Raman Spectroscopic Study

Michael D. Snodin, Lynda Ould-Moussa, Ursula Wallmann, Sophie Lecomte, Vinzenz Bachler, Eckhard Bill,* Helga Hummel, Thomas Weyhermüller, Peter Hildebrandt,* and Karl Wieghardt*[a]

Abstract: Hexadentate macrocyclic ligands containing a 1,4,7-triazacyclononane backbone and three N-bound pendent-arm phenolates form extremely stable neutral complexes with $Fe^{III}Cl_3$. The octahedral complexes $[Fe^{III}L]$ undergo three reversible one-electron oxidation processes to yield the mono- and dications, $[FeL]^+$ and $[FeL]^{2+}$, which are stable in solution for hours, whereas the trications, $[FeL]^{3+}$, are only stable in solution on the time scale of a cyclic voltammetric experiment. These oxidations are shown to be ligand- rather than metal-centered. Three coordinated phenoxyl radicals are formed successively as shown conclusively by Mössbauer spectroscopy. The neutral, mono-, di-, and tricationic species each contain an octahedral, high-spin ferric ion ($S_{Fe} = 5/2$), which is intramolecularly, antiferromagnetically coupled to the spin ($S = 1/2$) of the bound phenoxyl ligands to yield an $S_t = 2$ ground state for the monocation, and an $S_t = 3/2$ ground state for the dications as shown by EPR spectroscopy. The vibrations of the coordinated phenolate are observed by resonance Raman (RR) spectroscopy by excitation in resonance with the phenolate-to-iron charge-transfer (CT) transition above 500 nm or, alternatively, of the coordinated phenoxyl by excitation in resonance with the intraligand $\pi \rightarrow \pi^*$ transition at about 410 nm. Use of ^{18}O isotopomers selectively labeled at the phenolic oxygen allowed the identification of the C–O stretching and Fe–O stretching and bending modes. It is shown that the substitution pattern of phenolates and phenoxyls in their respective *ortho* and *para* positions and the charge of the complexes have a pronounced influence on the vibrational modes observed.

Keywords: iron · magnetic properties · Moessbauer spectroscopy · phenoxyl radicals · resonance Raman spectroscopy

Introduction

In a recent series of publications we have shown that phenoxyl radical transition metal complexes can be generated chemically, as well as photo- and electrochemically, by one-electron oxidation of the corresponding phenolato complexes [Eq. (1)].[1–8]

$$M^{n+}-O^{-}-R \xrightarrow{-e} M^{n+}-O^{\cdot}-R \qquad (1)$$

It was established that the stability of such phenoxyl radical complexes critically depends on the nature of the substitution pattern at the *ortho* and *para* positions of the phenolates in order to prevent bimolecular decomposition reactions. *tert*-Butyl and methoxy groups proved to be ideally suited for this purpose[3] because they decrease the oxidation potential of the phenolates and provide enough steric bulk to suppress bimolecular decay reactions. To date, only three complexes containing a coordinated phenoxyl have been isolated as crystalline solids, namely $[Ga^{III}L^{p\text{-}met}](ClO_4)$,[3] $[Fe^{III}L^{p\text{-}met}](ClO_4)$,[3] and $[Cr^{III}L^{p\text{-}met}](ClO_4)\cdot 3\,CH_3CN$,[2] where $H_3L^{p\text{-}met}$ represents the pendent-arm macrocycle 1,4,7-tris(3-*tert*-butyl-5-methoxy-2-hydroxybenzyl)-1,4,7- triazacyclononane.[3] The crystal structure of $[Cr^{III}L^{p\text{-}met}]\cdot(ClO_4)$ clearly revealed that one coordinated phenoxyl radical and two phenolate pendent arms of the macrocycle are bound to a chromium(III) center, thus rendering it distorted octahedral.[2] These radical complexes are of considerable interest as such species have been identified in the active sites of at least two copper-containing enzymes, namely, galactose oxidase[9] and glyoxal oxidase.[10]

The electronic structure of such species presents an intellectually interesting, fundamental problem since one-

[a] Dr. E. Bill, Dr. P. Hildebrandt, Prof. Dr. K. Wieghardt, Dr. M. D. Snodin, Dr. L. Ould-Moussa, Dr. U. Wallmann, Dr. S. Lecomte, Dr. V. Bachler, Dr. H. Hummel, Dr. T. Weyhermüller
Max-Planck-Institut für Strahlenchemie
Stiftstrasse 34–36, D-45470 Mülheim (Germany)
Fax: (+49) 208-306-3952
E-mail: wieghardt@mpi-muelheim.mpg.de

  0947-6539/99/0509-2554 $ 17.50+.50/0 *Chem. Eur. J.* **1999**, *5*, No. 9

electron oxidation of a phenolato transition metal complex can be either ligand- or metal-ion-centered. Therefore, chemists and spectroscopists must develop criteria by which one can unambiguously distinguish between these two possibilities. As it turns out, coordinated phenoxyl radicals display characteristic vibrational features that can be observed elegantly and selectively by resonance Raman (RR) spectroscopy.[4–8] Conversely, changes in the d^n electron configuration can be detected most readily by (i) X-ray absorption near-edge spectroscopy (XANES) by interrogating the transition metal K-edge energy of the reduced and oxidized forms,[9d] and, in the case of iron complexes, by (ii) Mössbauer spectroscopy, which is a very sensitive probe for oxidation state changes (or the lack thereof)[1, 3] at the iron center. In some cases EPR spectroscopy can reveal the spin ground state and the nature of the local spins involved and, hence, distinguish between metal-centered oxidations and ligand radical formation.

When we investigated the RR spectra of phenoxyl radical complexes[4–8] it became clear that the assignment of some vibrational modes (in particular, the ν_{7a} which is predominantly a ν(C–O•) stretching mode) was often difficult because of the lack of data on complexes with phenolates (and, upon oxidation, phenoxyls) that are ^{18}O labeled at the phenolic oxygen. In this paper we report the synthesis and characterization of some tris(phenolato)iron(III) complexes and their phenoxyl radical analogues. The series under investigation is shown in Scheme 1. We have been able to

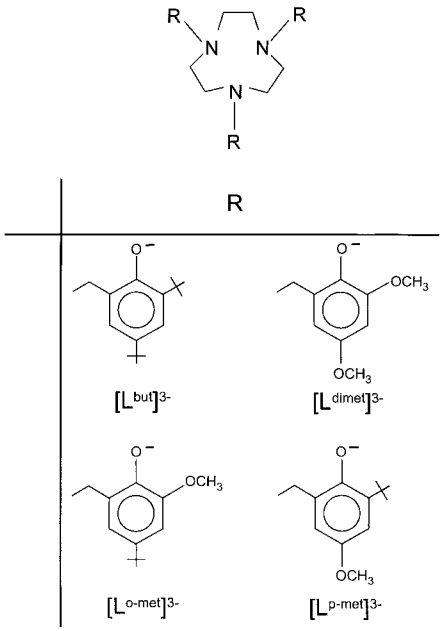

Scheme 1. Structures of the pendent-arm phenolate ligands.

prepare the selectively ^{18}O-labeled ligand H_3L^{dimet}, the complex $[Fe^{III}L^{dimet}]$, and its monocation $[Fe^{III}L^{dimet}]^+$ which contains a coordinated phenoxyl and two phenolato pendent arms. With zero- and applied-field Mössbauer and EPR spectroscopy we will show that the complexes contain exclusively high-spin ferric ions (d^5, $S = 5/2$).

Results

Syntheses: Preparation of the ligands H_3L^{but} and $H_3L^{p\text{-}met}$ has been described previously.[3] The new ligands H_3L^{dimet} and $H_3L^{o\text{-}met}$ have been synthesized accordingly by reaction of 1,4,7-triazacyclononane with three equivalents of the respective phenol (2,4-dimethoxyphenol, 2-methoxy-4-*tert*-butylphenol) and three equivalents of paraformaldehyde in methanol (Mannich reaction). The pendent-arm macrocycles have been isolated as sticky brown gums that were used for complex formation without further purification. Both ligands react quantitatively with one equivalent of $FeCl_3$ in methanol to afford red microcrystals of $[Fe^{III}L^{dimet}]$ and $[Fe^{III}L^{o\text{-}met}]$, respectively. The complexes $[Fe^{III}L^{but}]$ and $[Fe^{III}L^{p\text{-}met}]$ have been prepared and characterized previously.[3]

A ligand H_3L^{dimet}, selectively ^{18}O-labeled at the phenolic oxygen, and the complex $[Fe^{III}L^{dimet}]$ were prepared as described above from ^{18}O-labeled 2,4-dimethoxy phenol as the starting material. This precursor was synthesized by $^{18}O_2$ oxidation of the Grignard reagent obtained from a 1:1 mixture of 1-bromo-2,4-dimethoxybenzene and isopropyl bromide in dry tetrahydrofuran.

Crystal structure of $[Fe^{III}L^{dimet}]\cdot 2\,CH_3CN$: Slow recrystallization of $[Fe^{III}L^{dimet}]$ from a solution of the complex in acetonitrile produced red-purple single crystals of $[Fe^{III}L^{dimet}]\cdot 2\,CH_3CN$ that were suitable for X-ray crystallography. Table 1 summarizes selected bond lengths and angles. The

Table 1. Selected bond lengths [Å] and angles [°] of $[FeL^{dimet}]\cdot 2\,CH_3CN$.

Fe–O1	1.914(2)	Fe–O4	1.923(2)	Fe–O7	1.926(2)
Fe–N1	2.230(3)	Fe–N2	2.239(3)	Fe–N3	2.203(3)
O1–C9	1.330(4)	O4–C18	1.337(4)	O7–C27	1.331(4)
O3–C12	1.385(4)	O6–C21	1.387(4)	O9–C30	1.382(4)
O3–C15	1.421(4)	O6–C24	1.418(5)	O9–C33	1.423(4)
O1-Fe-O4	97.4(1)	O1-Fe-O7	98.6(1)	O7-Fe-N2	164.6(1)
O4-Fe-O7	98.2(1)	O1-Fe-N3	166.5(1)	N3-Fe-N2	78.2(1)
O4-Fe-N3	93.5(1)	O7-Fe-N3	87.7(1)	N1-Fe-N2	77.8(1)
O1-Fe-N1	88.3(1)	O4-Fe-N1	166.0(1)	C9-O1-Fe	132.7(2)
O7-Fe-N1	93.5(1)	N3-Fe-N1	79.4(1)	C18-O4-Fe	131.7(2)
O1-Fe-N2	93.9(1)	O4-Fe-N2	89.0(1)	C27-O7-Fe	133.5(2)

structure consists of well-separated, neutral $[Fe^{III}L^{dimet}]$ (Figure 1) and acetonitrile molecules of crystallization. The central iron(III) ion is in a distorted octahedral *cis* N_3O_3 donor environment. The Fe–O and Fe–N distances are much like those reported previously for similar complexes.[11] The Fe–O bonds are short and indicate significant double-bond character, whereas the Fe–N bonds are long. The average O-Fe-O bond angle of 98.9° is significantly larger than the ideal octahedral angle of 90°, which also indicates oxygen-to-iron π bonding. The average C_{phenyl}–$O_{phenolate}$ bond length of 1.333(4) Å is characteristic of coordinated phenolates. In coordinated phenoxyls this bond is shorter (1.290(4) Å), as has been determined crystallographically for $[Cr^{III}L^{p\text{-}met}](ClO_4)$,[2] which contains one phenoxyl and two phenolate ligands.

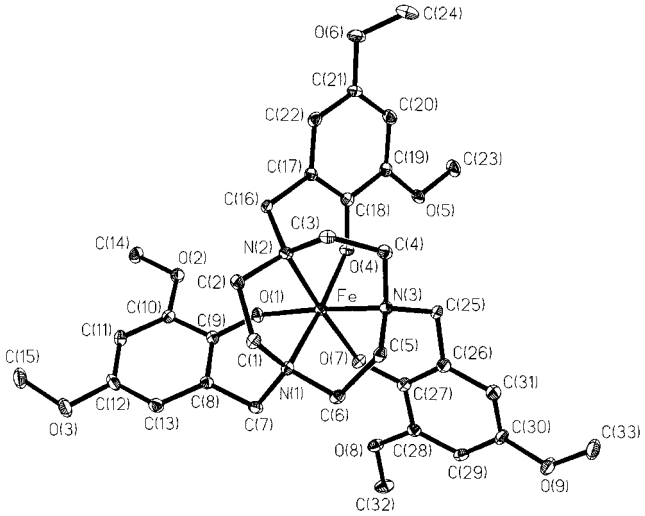

Figure 1. Crystal structure of $[FeL^{dimet}]$.

Electrochemistry: The electrochemistry of the neutral tris(phenolato)iron(III) complexes has been studied by cyclic voltammetry in CH_3CN and/or CH_2Cl_2 solutions with tetra-*n*-butylammonium hexafluorophosphate (0.10 M) as the supporting electrolyte; ferrocene was added as the internal standard. Table 2 summarizes the results; all redox potentials are referenced against the ferrocenium/ferrocene (Fc^+/Fc) couple.

All of the neutral complexes display very similar behavior. Three reversible one-electron oxidative waves and a single reversible one-electron reduction are observed in the potential range $+1.2$ to -2.0 V versus Fc^+/Fc. The oxidations are assigned to three successive ligand-centered, phenolate-to-phenoxyl oxidations [Eq. (2)], whereas the reduction wave corresponds to a metal-centered reduction $Fe^{III} \rightarrow Fe^{II}$, [Eq. (3)].

$$[Fe^{III}L]^0 \underset{+e}{\overset{-e(E^3)}{\rightleftharpoons}} [Fe^{III}L]^{+\cdot} \underset{+e}{\overset{-e(E^2)}{\rightleftharpoons}} [Fe^{III}L]^{2+\cdot\cdot} \underset{+e}{\overset{-e(E^1)}{\rightleftharpoons}} [Fe^{III}L]^{3+\cdots} \quad (2)$$

$$[Fe^{III}L]^0 \underset{-e}{\overset{+e(E^4)}{\rightleftharpoons}} [Fe^{II}L]^- \quad (3)$$

The mono- and dications are readily prepared electrochemically in solution by coulometry at an appropriately fixed potential; they are stable in solution at room temperature for a few hours and can therefore be characterized spectroscopically (UV/Vis, Mössbauer, EPR). The trications are unstable on this time scale and they decompose within minutes. The differences between the redox potentials E^1 and E^2, and E^2 and E^3 of a given species are nearly identical. This has been explained previously[3] by a simple electrostatic model that takes into account the difference in solvation energy of species carrying an n^+ and an $(n+1)^+$ charge. Two aspects of the results in Table 2 are remarkable.

1) The redox potentials for the ligand oxidations are clearly dependent on the substitution pattern of the coordinated phenolate. Thus $[FeL^{dimet}]$ is the most easily oxidized complex followed by $[FeL^{p\text{-}met}]$, $[FeL^{o\text{-}met}]$, and $[FeL^{but}]$. Obviously, the presence of a *p*-methoxyphenolate feature facilitates the oxidation to a greater extent than an *o*-methoxyphenolate.
2) In contrast, the metal-centered reduction Fe^{III}/Fe^{II} is virtually independent of the nature of the coordinated phenolates.

Table 2. Redox potentials[a] of complexes.

Complex	$E^1_{1/2}$ [b]	$E^2_{1/2}$	$E^3_{1/2}$	$E^4_{1/2}$	Solvent	Ref.
$[FeL^{but}]$	0.96(irr.)	0.65	0.38	−1.78	CH_3CN	[3]
$[FeL^{dimet}]$	0.46	0.28	0.11	−1.77	CH_2Cl_2	this work
$[FeL^{o\text{-}met}]$	0.71	0.50	0.30	−1.79	CH_2Cl_2	this work
$[FeL^{p\text{-}met}]$	0.63	0.38	0.14	−1.81	CH_3CN	[3]

[a] Conditions: [complex] $\approx 10^{-3}$ M in CH_3CN or CH_2Cl_2 (0.10 M $[nBu_4N]PF_6$, Ar atmosphere, $T = 298$ K, glassy carbon working electrode; reference electrode Ag/AgCl (saturated LiCl in ethanol); ferrocene internal standard; scan rate 200 mV s^{-1}. [b] The potentials are referenced versus the ferrocenium/ferrocene (Fc^+/Fc) couple: $E_{1/2} = (E_p^{ox} + E_p^{red})/2$ for reversible one-electron transfer processes; the oxidation peak potential, E_p^{ox}, is given for the irreversible process.

Electronic structure: All neutral tris(phenolato)iron(III) complexes contain an octahedral high-spin ferric ion (d^5), which gives rise to a temperature-independent magnetic moment of 5.9 Å $\pm$ 0.1 μ_B (Table 3). Their electronic spectra are dominated by an intense ($\varepsilon > 10^3$) phenolato-to-iron charge transfer (CT) band in the visible (500–525 nm) and by two phenolate $\pi \rightarrow \pi^*$ and $n \rightarrow \pi^*$ transitions at < 300 nm. In some cases a shoulder at ≈ 330 nm is detected, which may come from an amine-to-iron(III) CT band. The spectra of the electrochemically generated monocations $[FeL^{but}]^+$,

Table 3. Electronic spectra (CH_3CN) and magnetic properties of complexes.

Complex	λ_{max} [nm] (ε[L mol^{-1} cm^{-1}])	μ_{eff} (295 K)[μ_B]	Ref.
$[FeL^{but}]$	244 (2.5×10^4), 287 (1.8×10^4), 330sh (1.0×10^4), 500 (8.4×10^3)	5.9	[3]
$[FeL^{but}]^+$ [a]	248sh (1.5×10^4), 298 (1.4×10^4), 344 (7.5×10^3), 406 (4.6×10^3), 564 (4.8×10^3)		this work
$[FeL^{dimet}]$	245 (2.3×10^4), 299 (1.7×10^4), 523 (8.1×10^3)	5.9	this work
$[FeL^{dimet}]^+$ [a]	244 (2.0×10^4), 304 1.9×10^4), 420 (9.9×10^3), 612 (7.0×10^3)		this work
$[FeL^{o\text{-}met}]$	245 (2.7×10^4), 290 (1.8×10^4), 316sh, 512(9.5×10^3)	5.9	this work
$[FeL^{o\text{-}met}]^+$ [a]	244 (2.3×10^4), 290(1.9×10^4), 396 (8.0×10^3), 582 (7.0×10^3)		this work
$[FeL^{o\text{-}met}]^{2+}$	244sh, 288 (2.1×10^4), 404 (1.2×10^4), 656 (6.0×10^3)		this work
$[FeL^{p\text{-}met}]$	245 (2.2×10^4), 303 (2.1×10^4), 513 (8.9×10^3)	5.9	[3]
$[FeL^{p\text{-}met}]^+$ [a]	241 (2.0×10^4), 302 (2.2×10^4), 332sh (1.2×10^4), 402sh (7.8×10^3) 421 (1.0×10^4), 562 (6.7×10^3)		[3]
$[FeL^{p\text{-}met}]^{2+}$ [a]	244 (2.0×10^4), 300 (2.2×10^4), 332 (1.4×10^4), 431 (1.8×10^4), 610 (6.5×10^3), 750sh (5.0×10^3)		[3]

[a] CH_2Cl_2; electrochemically generated (0.10 M $[nBu_4N]PF_6$).

0947-6539/99/0509-2556 $ 17.50+.50/0 *Chem. Eur. J.* **1999**, *5*, No. 9

$[FeL^{dimet}]^+$, $[FeL^{o\text{-}met}]^+$, and $[FeL^{p\text{-}met}]^+$ are also very similar. Most importantly, the new intense band at $\approx 400 \pm 20$ nm is indicative of phenoxyl radical formation.[3] In the corresponding dications the intensity of this absorption is twice as large as in the monocations. Note that the neutral complexes show no absorption at 400 nm. The phenolate-to-iron(III) CT band in the visible region is also affected by the successive oxidation of one and two coordinated phenolates to phenoxyls: the intensity decreases somewhat and the maximum is successively shifted to lower energies, as is shown for the mono- and dication of $[Fe^{III}L^{dimet}]$ in Figure 2.

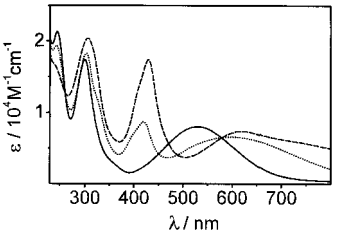

Figure 2. Absorption spectra of $[FeL^{dimet}]$ (solid), $[FeL^{dimet}]^{+\bullet}$ (dotted), and $[FeL^{dimet}]^{2+}$: (broken) in CH_2Cl_2/ tBu_4NPF_6.

Zero-field Mössbauer spectra: The fact that oxidation of neutral complexes involves the coordinated phenolates, and *not* the metal ion (no Fe^{IV}!), is proven by Mössbauer spectroscopy. We measured spectra at 80 K of the solid $[Fe^{III}L]$ complexes and their ^{57}Fe-enriched (35%) mono- and dications in frozen acetonitrile solution. The results are summarized in Table 4.

Table 4. Zero-field Mössbauer spectra of complexes at 80 K.

Complex	δ [a] [mm s^{-1}]	ΔE_Q [mm s^{-1}]	Ref.
$[FeL^{but}]$	0.49	0.83	[3]
$[FeL^{but}]^{+}$ [b]	0.53	1.08	this work
$[FeL^{dimet}]$	0.53	0.61	this work
$[FeL^{dimet}]^{+}$ [b]	0.52	0.95	this work
$[FeL^{o\text{-}met}]$	0.47	0.50	this work
$[FeL^{o\text{-}met}]^{+}$ [b]	0.51	0.97	this work
$[FeL^{p\text{-}met}]$	0.52	0.63	[3]
$[FeL^{p\text{-}met}](ClO_4)$ [b]	0.54	0.95	[3]
$[FeL^{p\text{-}met}]^{2+}$	0.54	1.09	this work

[a] Referenced vs. α-Fe at ambient temperature. [b] Electrochemically generated, measured in frozen CH_2Cl_2 solution containing ^{57}Fe-enriched samples.

The spectra of the neutral complexes consist of broadened quadrupole doublets that were approximately fitted with Lorentzian lines. The fits yielded isomer shifts in the narrow range of 0.47 – 0.53 mm s^{-1} and small quadrupole splittings of 0.50 – 0.83 mm s^{-1}. These values are typical of octahedral, high-spin ferric complexes. Similarly, for the monocations $[FeL]^+$ isomer shifts of 0.51 – 0.54 mm s^{-1} and quadrupole splittings in the range of 0.95 – 1.08 mm s^{-1} are again indicative of the presence of high-spin iron(III). In contrast, the isomer shifts of octahedral Fe^{IV} complexes (characterized by the $3d^4$ configuration; $S = 1$ or 2) are found in the range 0.09 – 0.23 mm s^{-1}.[12–23] The Mössbauer parameters for the dication $[FeL^{p\text{-}met}]^{2+}$ of $\delta = 0.54$ mm s^{-1} and $\Delta E_Q = 1.09$ mm s^{-1} indicate that even a two-electron oxidation of neutral $[FeL^{p\text{-}met}]$ cannot be metal-centered. The dication $[FeL^{p\text{-}met}]^{2+}$ also contains a high-spin ferric ion.

Both the neutral complexes and the dications show very broad Mössbauer absorptions with non-Lorentzian line shapes when measured in zero or weak field at $T = 2$ – 200 K; in *frozen solution* the spectra of the neutral complexes are completely smeared out. In contrast, the monocations exhibit well-resolved quadrupole spectra with narrow Lorentzian lines. This effect originates from the fundamental difference between Kramers and non-Kramers systems (odd number of electrons and half-integer spin versus even number of electrons and integer spin, respectively). Kramers systems have sizeable spin expectation values $\langle \boldsymbol{S} \rangle$ and internal magnetic fields even in the absence of external fields. The observed broad lines of $[Fe^{III}L]$ and $[Fe^{III}L]^{2+}$ indicate the presence of such internal fields, which in our case are nonstationary because of intermediate spin relaxation.[24] For non-Kramers systems like the monocations the spin expectation values are zero without applied fields, and consequently, the Mössbauer spectra show quadrupole doublets at any temperature.[25] The collapse of the magnetic hyperfine splittings and the appearance of resolved quadrupole doublets for the neutral complexes *in the solid* at elevated temperatures (80 – 200 K) owe their origin to enhanced (intermolecular) spin-spin interactions in the crystals.

EPR and magnetic Mössbauer spectra: The electronic structures of the neutral and oxidized complexes were investigated further by studying the paramagnetic properties of $[FeL^{p\text{-}met}]^{0/+1/+2}$. X-band EPR spectra were recorded at 3 and 10 K and magnetic Mössbauer spectra were measured with applied fields of 0 – 7 T. For both techniques aliquots of the same ^{57}Fe-enriched sample (35%) in acetonitrile (1.5 mM) were used. The results of the spin Hamiltonian simulations are given in Table 5.

The neutral complex $[Fe^{III}L^{p\text{-}met}]$ displays rather broad EPR signals at $g = 4.3$ and $g \approx 9$ with additional weak features at higher field. The pattern is typical of $S = 5/2$ with rhombic symmetry ($E/D = 0.33$) and a small D parameter, being in the

Table 5. Spin Hamiltonian and Mössbauer parameters of $[FeL^{p\text{-}met}]^{n+}$.

Complex	S_t	D_t	D [a] [cm^{-1}]	E/D_t ($=E/D$ [a])	$A_t/g_N\mu_N$ T	A_{Fe} [a]	ΔE_Q [b] [mm s^{-1}]	η	δ [b] [mm s^{-1}]
$[Fe^{III}L^{p\text{-}met}]^0$	5/2	–	0.09[c]	0.33	–	– 21.4	+ 0.59	0	0.54
$[Fe^{III}L^{p\text{-}met}]^{1+}$	2	0.46	0.35	0.28	– 24.5	– 21.0	– 0.99[d]	0.7	0.53
$[Fe^{III}L^{p\text{-}met}]^{2+}$	3/2	0.51	0.27	0.07	– 29.1	– 20.8	– 1.20	0.1	0.56

[a] Intrinsic value of ferric iron. [b] Determined at 2 K. [c] Sign without physical meaning because of $E/D = 1/3$. [d] The efg is rotated by 90° around the z axis with respect to the principal axes system of the zero-field interaction.

order of hν ($\approx$0.3 cm^{-1}). We refrained from simulations of the spectra because signal distortions indicate perturbations from intermolecular spin–spin interactions even in dilute solutions.[26]

For the monocation $[FeL^{p\text{-}met}]^{+}$ a perpendicular-mode EPR spectrum was obtained which exhibits weak integer-spin resonances over a wide field range of 30–800 mT. The spectrum was partly obscured by superimposed prominent signals at $g = 4.3$ from unoxidized ferric starting material and a free-radical signal at $g = 2$. However in measurements with parallel-mode detection ($B_1 \parallel B_0$) the contaminant spectra were completely attenuated and the integer-spin spectra were significantly enhanced. Resonances are predominantly observed at weak fields with a dominant trough at 90 mT and an extremely broad, shallow absorption line at 200–400 mT. Spin Hamiltonian simulations for $S_t = 2$ approximate to these features when the zero-field splitting (ZFS) parameters for the total molecular spin are $0.4\ \text{cm}^{-1} < D_t < 0.6\ \text{cm}^{-1}$ and $E/D_t = 0.28$, where E/D_t was fixed to the value found from the Mössbauer simulations given below.

The dication $[FeL^{p\text{-}met}]^{2+}$ clearly showed a system spin ground state of $S_t = 3/2$ with an EPR derivative-signal at $g \approx 4$ and a broad trough close to $g = 2$, which is typical of resonances from a $|3/2, \pm 1/2\rangle$ in axial symmetry ($E/D_t \approx 0$). From simulations we estimate a ZFS parameter $D_t \leq 0.5\ \text{cm}^{-1}$. The Mössbauer sample of the monocation in solution contained 13% of the unoxidized neutral compound, and that of the dication contained 18% of the monocation. In both cases the contaminants were removed from the experimental data by subtracting the corresponding spectra measured under the same conditions. The magnetic spectra in Figure 3 show the corrected experimental data together with spin

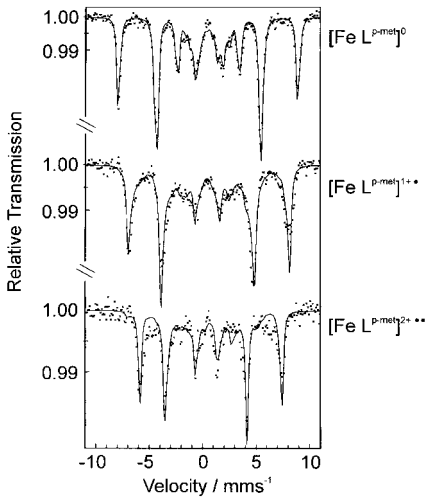

Figure 3. Magnetic Mössbauer spectra of $[FeL^{p\text{-}met}]^{n}$ in different oxidation states ($n = 0, +1, +2$) measured at 2 K with a field of 1 T applied perpendicular to the γ-beam.

Hamiltonian simulations [see Eqs. (4),(5)] with effective spins according to the respective ground states. The solid lines are the result of a least-squares optimization with a downhill simplex procedure performed simultaneously for at least three spectra recorded at different fields. The results are given in Table 5.

The Mössbauer spectra of neutral $[Fe^{III}L^{p\text{-}met}]$ in acetonitrile at 2 K with applied fields of 1,3,5, and 7 T show large splittings of about 16 mm s^{-1} that correspond to a strong internal field of about 53 T, which is as expected for ferric high-spin ions[27]. The spectra were simulated ($S = 5/2$) with an isotropic hyperfine coupling constant of $A_{Fe}/g_N\mu_N = -21.4$ T as shown in Figure 3 (top). Since the EPR spectra showed rhombic signals the rhombicity parameter was kept constant at $E/D = 0.33$ and the g value was fixed at 2. From the simulations we obtained an isomer shift for the compound in solution of $\delta = 0.54$ mm s^{-1} at 2 K and a quadrupole splitting of $+0.59$ mm s^{-1} with an asymmetry parameter of zero. The ZFS, which is mainly determined from the field dependence of the internal field, was found to be $D = 0.09\ \text{cm}^{-1}$, in accordance with previous magnetic susceptibility measurements[3] on the solid, which yielded an upper limit of $D < 0.5\ \text{cm}^{-1}$. Because of this small ZFS it was necessary to evaluate the spectra not only in strong but also in moderate and weak fields. The minimum field used in this study was 1 T. Below this field strength the spectra were obscured by relaxation effects, even in solution.

For solid $[FeL^{p\text{-}met}]^{+}[ClO_4]^{-}$ it has been shown by temperature-dependent magnetic susceptibility measurements that the monocation possesses an $S = 2$ ground state[3] as a result of strong intramolecular antiferromagnetic coupling between the ferric ion ($S = 5/2$) and the coordinated phenoxyl radical ($S = 1/2$). A coupling constant J of $-80\ \text{cm}^{-1}$ ($H = -2JS_1 \cdot S_2$; $S_1 = 1/2$; $S_2 = 5/2$) has been determined. The magnetic Mössbauer spectra, as well as the EPR spectra, which were obtained at liquid helium temperatures for *solutions* of the monocation, confirm the spin quintet ground state. Figure 3 (middle) shows the spectrum at 1 T field. The spin Hamiltonian simulations at 1,3, and 7 T yielded ZFS parameters for the ground state of $D_t = +0.46\ \text{cm}^{-1}$ and $E/D_t = 0.28$.

The effective quadrupole shifts in the magnetic six-line pattern of the monocation are apparently very small ($\approx$0.1 mm s^{-1}) by comparison with the quadrupole splitting of the zero-field spectrum of about 1 mm s^{-1}. Consistency of the simulations for the magnetic spectra with the zero-field result was achieved by adopting a large asymmetry parameter η and a rotation of the electric field gradient (efg) tensor with respect to the principal axes system of the ZFS. Then a very small component of the efg could be aligned along the direction of the internal field which, in first order, is exclusively effective for the magnetic pattern. Finite values of the asymmetry parameter reduce the efg component V_{xx} with respect to V_{yy} and V_{zz} by up to $\eta = 1$ when V_{xx} reaches zero. The internal field, however, is predominantly oriented in the y direction for the lowest, mainly populated Kramers doublet. We therefore introduced an Euler rotation of the efg around the z axis by an angle γ of 90° in order to orient $V_{x'x'}$ also in the y direction[28]. With this assumption simulations were possible with $\Delta E_Q = -0.99$ mm s^{-1} in accord with the 80 K zero-field spectra. The fits yielded an asymmetry parameter of $\eta = 0.7$.[29] We are aware that this is not necessarily a unique fit as additional, more complicated Euler rotations of the efg might prevail. However, the essential features of the quadrupole interaction for the ^{57}Fe site in the monocation are correctly described.

0947-6539/99/0509-2558 $ 17.50+.50/0 *Chem. Eur. J.* **1999**, *5*, No. 9

The magnetic ^{57}Fe hyperfine splittings for the monocation were reproduced with an isotropic effective hyperfine coupling constant for the ground state $S_t = 2$. The obtained value $A_t/g_N\mu_N = -24.5$ T is in accord with that found for the neutral complex if it is converted to the intrinsic representation $A_{Fe}/g_N\mu_N = -21.0$ T for $A_{Fe} = \frac{7}{7}A_t$. This equation is derived from spin projection for a coupled system of ferric iron ($S = 5/2$) and a radical ($S' = 1/2$). In the same coupling model, the ZFS parameter can be converted to a local iron value with $D = \frac{3}{4}D_t$ to yield $D = 0.35$ cm^{-1} and $E/D = 0.28$.

The Mössbauer spectra of the electrochemically generated diradical $[FeL^{p\text{-}met}]^{2+}$ in acetonitrile showed about 18% contamination by the monoradical precursor. Its contribution was again subtracted from the experimental data as descibed above. The magnetically perturbed spectra recorded at 2 K with fields of 1,3,5, and 7 T were readily simulated with the effective spin Hamiltonian [see Eq. (4)] for an energetically well isolated $S_t = 3/2$ ground state. The 1 T spectrum is shown as an example in Figure 3 (bottom). The fits gave the ZFS parameters $D_t = 0.51$ cm^{-1} and $E/D_t = 0.07$ in accordance with EPR measurements (intrinsic value $D = 0.27$ cm^{-1} when dipolar contributions to D_t are negligible). The quadrupole splitting ΔE_Q at 2 K was found to be -1.20 mm s^{-1} and the asymmetry of the efg practically vanishes (0.25 error limit for η). Again an isotropic effective hyperfine coupling constant was determined $A_t/g_N\mu_N = -29.1$ T, which yields $A_{Fe}/g_N\mu_N = -20.8$ T, when converted to the intrinsic value with $A_{Fe} = \frac{5}{7}A_t$ for the $|S^*S_t\rangle = |1,3/2\rangle$ ground state.

Interpretation of the spin Hamiltonian and Mössbauer parameters: The Mössbauer isomer shifts of the compounds under investigation prove that the iron is in a ferric high-spin state and, hence, that the complex oxidations are ligand-centered. Furthermore, the isomer shift δ is virtually independent of oxidation state for complexes $[FeL]^{n+}$ with the same ligand L. Since δ depends on the occupation of iron s and d orbitals[24, 30] we conclude that the overall covalency of the iron–ligand bonds is independent of ligand oxidation. This is in contrast to what one might expect, if back bonding, for instance, were enhanced upon removal of a ligand electron. For comparison, the variation in isomer shift of octahedral ferric high-spin complexes with different covalencies, like $FeCl_3$ ($\delta = 0.49$ mm s^{-1}) and $Fe_2(SO_4)_3$ ($\delta = 0.39$ mm s^{-1}), is of the order -0.1 mm s^{-1}.[27] In our case, if there is a trend in isomer shifts for the complexes $[Fe^{III}L]^{n+}$, it is perhaps a slight increase in the numerical values on oxidation by about $+0.02$ mm s^{-1} rather than a decrease (see Tables 4 and 5).

A similar conclusion can be drawn from the small variation in the magnetic hyperfine coupling constant A of $[Fe^{III}L^{p\text{-}met}]^{n+}$ summarized in Table 5. The A values depend on the density of *unpaired* spin in the iron s and d orbitals. In general, A tends to decrease with increasing covalency,[31] as does the isomer shift. Whether the small (3%) decrease in A in the series $[Fe^{III}L^{p\text{-}met}]^0$ to $[Fe^{III}L^{p\text{-}met}]^{2+}$ really reflects increased covalency can not be decided at this point. An interesting alternative explanation would be a direct exchange polarization of iron s electrons by the minority spin in the covalently bound ligand orbitals. Such a mechanism has been discussed for delocalized minority spin density in nonradical complexes.[32]

On the basis of structural considerations we explain the oxidation invariance of the overall covalency by a compensation effect of the weakening of the $Fe{-}O_{phenoxyl}$ bond upon formation of the radical and the concomitant strengthening of the remaining $Fe{-}O_{phenolate}$ bonds. Such behavior was recognized previously in the molecular structures of similar Cr^{III} complexes.[2] The RR studies discussed below confirm that the same structural variations in Fe–O bonds prevail for the complexes presented here.

Covalency is the major source of the electric field gradient (efg) at the iron nucleus of ferric compounds, as the valence contribution to the efg from a spherical, half-filled $3d^5$ shell of a hypothetical ionic compound would vanish.[24, 30] Large electric quadrupole splittings of more than 1 mm s^{-1} are known to occur for $Fe^{III}_2(\mu\text{-oxo})$ dimers.[16, 17, 33, 34] It is the asymmetry in 3d occupation due to the short covalent Fe–oxo bond which gives rise to the large efg.

The relatively small quadrupole splitting of the neutral complexes in this study corresponds to the high symmetry of ferric iron in a trigonal moiety with small axial distortion. The positive sign of the efg main component V_{zz} implies excess electronic charge in the equatorial plane and, interestingly, correlates with a slight axial compression of the coordination polyhedron of the iron, as determined by X-ray diffraction.

The significant elongation of one Fe–O bond upon one-electron oxidation that can be anticipated from our previous results,[2] perturbs significantly the trigonal iron coordination symmetry. The asymmetry is further enhanced by the supposed shortening of the remaining $Fe{-}O_{phenolate}$ bonds.[2] The resulting *difference* in covalent delocalization of the different 3d orbitals gives rise to a large efg as is observed for the monoradicals. The large asymmetry parameter η reflects the local C_s symmetry.

The dication $[FeL^{p\text{-}met}]^{2+}$ supposedly has two weak $Fe{-}O_{phenoxyl}$ bonds and one strong $Fe{-}O_{phenolate}$ bond, and the small asymmetry parameter suggests that this arrangement takes essentially octahedral coordination symmetry with only weak tetragonal distortion. The large V_{zz} component would be consistent with a covalent Fe–O bond in the z direction, and with two Fe–O and two Fe–N bonds with rather weak covalency in the equatorial plane.

Resonance Raman spectroscopy

Tris(phenolato)iron(III) complexes: Figures 4 and 5 display the RR spectra of the parent complexes $[FeL^{but}]$, $[FeL^{p\text{-}met}]$, $[FeL^{o\text{-}met}]$, and $[FeL^{dimet}]$ excited in resonance with the phenolate-to-iron charge-transfer transition. These species differ in the substitution pattern of the phenolate rings, that is, *tert*-butyl and methoxy substituents in the *ortho* and *para* positions. In the high frequency region (Figure 4), all of the spectra display a prominent band at about 1600 cm^{-1} that is readily assigned to the ν_{8a} mode according to Wilson's notation adapted to substituted benzenes.[35] This mode includes predominantly the C=C stretching coordinates (C_{ortho}=C_{meta}), as suggested from previous normal mode analyses.[35–37] This assignment is in line with the fact that

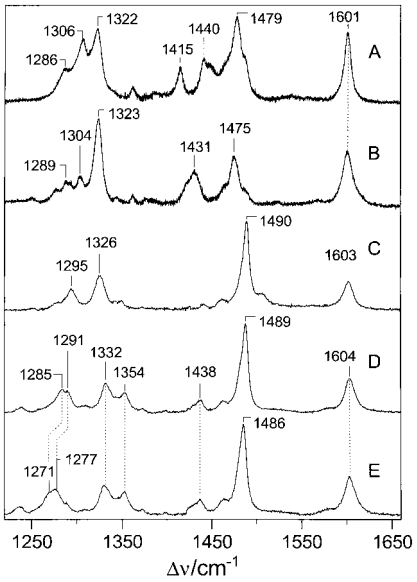

Figure 4. RR spectra of (**A**) [FeL^{but}], (**B**) [FeL$^{p\text{-}met}$], (**C**) [FeL$^{o\text{-}met}$], (**D**) [FeL^{dimet}], and (**E**) the ^{18}O-labeled [FeL^{dimet}]. The excitation wavelengths were 571 (**A**, **B**) and 514 nm (**C**, **D**, and **E**). The Raman bands of the solvent (**A**, **B**: $CH_3CN/LiClO_4$; **C**, **D**, and **E**: CH_2Cl_2/ tBu$_4$NPF$_6$) are subtracted.

^{18}O labeling of the phenolate oxygen does not produce a frequency shift of this band, thus ruling out any contribution from the C–O stretching coordinate. Below 1500 cm^{-1} we note substantial differences between the species carrying a *tert*-butyl and a methoxy group at the *ortho* positions of the phenolates. Evidently, the internal vibrations of the *ortho* substituents mix to a considerable extent with the phenolate ring vibrations. On the other hand, the *para* substituent has a less pronounced effect on the vibrational band pattern, since the RR spectra of [FeL^{but}] and [FeL$^{p\text{-}met}$] are similar to those of [FeL$^{o\text{-}met}$] and [FeL^{dimet}].

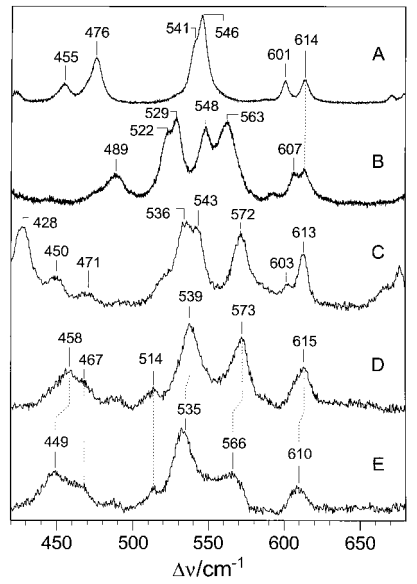

Figure 5. RR spectra of (**A**) [FeL^{but}], (**B**) [FeL$^{p\text{-}met}$], (**C**) [FeL$^{o\text{-}met}$], (**D**) [FeL^{dimet}], and (**E**) the ^{18}O-labeled [FeL^{dimet}]. The excitation wavelengths were 571 (**A**, **B**) and 514 nm (**C**, **D**, and **E**). The Raman bands of the solvent (**A**, **B**: $CH_3CN/LiClO_4$; **C**, **D**, and **E**: CH_2Cl_2/TBAPF$_6$) are subtracted.

Comparison of the RR spectrum of [FeL^{dimet}] with that of the ^{18}O-labeled derivative identifies modes that include contributions from the C–O stretching coordinate. The main shifts are observed for the closely spaced bands at 1291 and 1285 cm^{-1}, which both shift down by about 14 cm^{-1}. These shifts suggest that both modes have predominantly C–O stretching character. Their frequencies are close to that of the ν_{7a} mode of uncoordinated phenolates,[35–37] which implies that in tris(phenolato)iron(III) complexes this mode splits into two components. In fact, because of the C_{3v} symmetry of [FeL^{dimet}] one would expect two ν_{7a}-like modes (A_1 and E). A smaller shift to lower energy by 3 cm^{-1} is observed for the band at 1489 cm^{-1}, which is therefore assigned to the mode ν_{19a} for which normal mode analyses predict some C–O stretching character.[35–37] Minor frequency shifts (<3 cm^{-1}) for the bands at 1240 and 1332 cm^{-1} imply that the underlying modes also include some contributions from the C–O stretch. The frequency shifts observed for the modes ν_{7a} and ν_{19a} are in qualitative agreement with a recent study on uncoordinated phenolate by Mukherjee et al.[35] These authors used an empirical force field, fitted to the experimental data for phenolate as well as their deuterated and ^{13}C-labeled isotopomers. Based on this force field they calculated the normal modes for the ^{17}O-labeled phenolate yielding shifts of -5 and -3 cm^{-1} for the modes ν_{7a} and ν_{19a}, respectively. On the other hand, quantum chemical force field calculations carried out in this work predict essentially the same ^{18}O/^{16}O shifts for these modes (Table 6), indicating an overestimation of the C–O stretching contribution to the ν_{19a}. This discrepancy is due to the failure of the quantum chemical methods to describe the excess electron density adequately.[8, 37, 38]

Based on the present unambiguous identification of the band at 1489 cm^{-1} of [FeL^{dimet}] as the mode ν_{19a}, the respective bands at 1478 and 1475 cm^{-1} of [FeL^{but}] and [FeL$^{p\text{-}met}$] are now reassigned to this mode, thereby revising any previous suggestions.[8] For this mode in the various complexes, we note that the frequencies are lower for those complexes with a *tert*-butyl group at the *ortho* position compared with the methoxy-substituted complexes.

In the low-frequency region (Figure 5), strong Raman bands of the solvent (CH_2Cl_2) obscur the RR bands of the complexes between 680 and 760 cm^{-1}. Below 680 cm^{-1}, comparison of the RR spectra of the ^{16}O- and ^{18}O-labeled [FeL^{dimet}] reveals isotopic shifts of four bands, namely, 615 (-5), 573 (-7), 539 (-4), and 458 (-9) cm^{-1}. Normal mode analyses of uncoordinated phenolates predict two ^{18}O/^{16}O-sensitive bands at 511 (-9) and 430 (-11) cm^{-1}, which originate from a ring deformation (ν_{6a}) and the CO bending vibration (Table 6). Hence, these two modes are assigned to the bands observed at 539 and 458 cm^{-1}, respectively. In addition, one expects an Fe–O stretching vibration which in related compounds has been identified at ca. 600 cm^{-1}.[39, 40] As the spectra of [FeL^{dimet}] reveal two ^{18}O/^{16}O-sensitive bands in this region, we conclude that both modes include a substantial contribution from the Fe–O stretching coordinate. In fact, the isotopic shift of each band is smaller than that expected for a pure Fe–O stretch. Conversely, this conclusion implies that the Fe–O stretching coordinate is coupled with

  0947-6539/99/0509-2560 $ 17.50+.50/0 *Chem. Eur. J.* **1999**, *5*, No. 9

Table 6. Frequencies of selected phenolate and phenoxyl modes.[a]

Mode	ν_{19a}	ν_{7a}	$\nu_{Fe-O}(1)$	$\nu_{Fe-O}(2)$	ν_{6a}	δ_{CO}
			Phenolate			
$PheO^-$ (exp.)[b]	1534	1264	–	–	–	–
$PheO^-$ (calc.)[c]	1501(−12)	1355(−10)	–	–	511(−9)	430(−11)
$[FeL^{dimet}]$	1489(−3)	1291(−14)	615(−5)	573(−7)	539(−4)	458(−9)
		1285(−14)				
$[FeL^{p\text{-}met}]$	1475	1289	614	563	529	–
		1275				
$[FeL^{o\text{-}met}]$	1490	1295	613	572	536	455
$[FeL^{but}]$	1478	1286	614	–	546	418
$[FeL^{dimet}]^{+\cdot}$	1484(−1)	1274(−9)	616(−4)	578(−7)	542(−3)	462(−8)
$[FeL^{p\text{-}met}]^{+\cdot}$	1468	1278	614	570	538	–
$[FeL^{but}]^{+\cdot}$	1470	1280	615	–	551	451
			Phenoxyl			
p-$CH_3OPheO^{\cdot}$ (exp.)	1406	1518	–	–	–	–
p-$CH_3OPheO^{\cdot}$ (calc.)[c]	1409(−10)	1492(−6)	–	–	514(−3)	436(−8)
$[FeL^{dimet}]^{+\cdot}$	1499(−17)	1517(−4)	–	–	–	–
$[FeL^{o\text{-}met}]^{+\cdot}$	–	1519	–	–	–	–
$[FeL^{p\text{-}met}]^{+\cdot}$	1488	1501	586	–	527	419

[a] Frequencies are given in cm^{-1}; the $^{18}O/^{16}O$ shifts are given in parenthesis. [b] Taken from ref. [19]. [c] Calculated frequencies as obtained by DFT(B3LYP) were multiplied by 0.9744.[8]

ligand vibrations as has also been found for Fe–catecholate complexes.[38]

By comparing the low-frequency RR spectra of $[FeL^{dimet}]$ with those of the other Fe–phenolate species, we note that the vibrational band pattern appears to depend on both the *ortho* and the *para* substituent, since there are no strong spectral similarities, for instance, between $[FeL^{but}]$ and $[FeL^{p\text{-}met}]$. Thus, unambiguous identification of the C–O bending vibrations of these complexes is not possible without $^{18}O/^{16}O$ labeling. The effect of the substitution pattern on the other $^{18}O/^{16}O$-sensitive bands seems to be more systematic. Whereas the 615 cm^{-1} band remains largely unchanged in all complexes, the counterparts of the other Fe–O stretching mode of $[FeL^{dimet}]$ at 573 cm^{-1} can be attributed to the bands at 572 and 563 cm^{-1} in the *para*- and *ortho*-methoxy substituted complexes, respectively. Similarily, one may relate ν_{6a} of $[FeL^{dimet}]$ at 539 cm^{-1} to the bands at 536 and 529 cm^{-1} of $[FeL^{o\text{-}met}]$ and $[FeL^{p\text{-}met}]$, respectively. However, for these two complexes additional bands in this region (apparently due to the more asymmetric substitution pattern) make these correlations less unambiguous. In contrast, the RR spectrum of the di-*tert*-butyl substituted phenolate complex displays only one prominent peak at 546 cm^{-1}, which, however, has an asymmetric bandshape. Thus, it may be that in this case the band at 573 cm^{-1} is shifted down so that it nearly coincides with the ν_{6a} band. These findings imply that the separation of those modes, which in $[FeL^{dimet}]$ include the Fe–O stretch, depends on the substitution pattern of the phenolates. Hence, the relative contribution of this coordinate to these modes may vary substantially among the various complexes. In particular, it may be that the band at 614 cm^{-1} in $[FeL^{but}]$ is a largely pure Fe–O stretching as suggested previously.[8]

Phenoxyl radical complexes of iron(III): Figure 6 shows the RR spectra of the radical complex $[FeL^{dimet}]^{+\cdot}$ upon excitation in resonance with the $\pi \rightarrow \pi^*$ transition at $\approx$410 nm. The most pronounced $^{18}O/^{16}O$-isotopic shift is expected for the band at 1517 cm^{-1}, which in related complexes has been assigned to

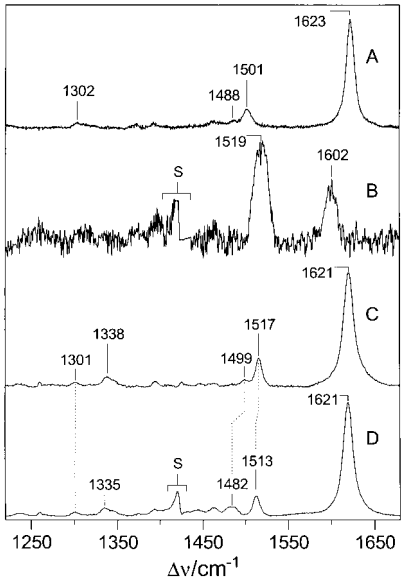

Figure 6. RR spectra of (**A**) $[FeL^{p\text{-}met}]^{+\cdot}$, (**B**) $[FeL^{o\text{-}met}]^{+\cdot}$, (**C**) $[FeL^{dimet}]^{+\cdot}$, and (**D**) the ^{18}O-labeled $[FeL^{dimet}]^{+\cdot}$. The excitation wavelengths were 418 (**A**) and 413 nm (**B**, **C**, and **D**). The Raman bands of the solvent (**A**: $CH_3CN/LiClO_4$; **B**, **C**, and **D**: CH_2Cl_2/t-Bu_4NPF_6) are subtracted. S denotes a subtraction artifact.

the mode ν_{7a} with predominantly C–O stretching character.[8] The 4 cm^{-1} shift to lower energy, however, is smaller than that of the adjacent band at 1499 cm^{-1}, which is found at 1482 cm^{-1} in the ^{18}O-labeled compound. This latter band is attributed to the mode ν_{19a}, which, according to normal mode analyses, should also exhibit a contribution from the C–O stretch.[35, 37] However, the distribution of the C–O stretching coordinate is simply reversed compared with the uncoordinated phenoxyl radicals where ^{17}O labeling yields shifts of −13 and −8 cm^{-1} for the modes ν_{7a} and ν_{19a}, respectively. Coordination to the iron center leads to a redistribution of the C–O stretching coordinate mainly among the modes ν_{7a} and ν_{19a}, although, to a minor extent, adjacent modes may also include some C–O

stretching contributions as reflected by the small isotopic shifts of the bands at 1448 and 1338 cm^{-1}. In view of these findings, it may well be that the composition of the modes ν_{7a} and ν_{19a} also depends on the kind of the coordinated metal ion. Nevertheless, it is possible to extend these assignments to related radical complexes.[8] Thus, the mode ν_{19a} is then reassigned to the bands observed between 1480 and 1495 cm^{-1}, for example, to that at 1488 cm^{-1} in $[FeL^{p\text{-}met}]^{+\cdot}$ (Figure 6).

In addition, comparison of the RR spectra in Figure 6 shows that the substitution pattern has a pronounced effect on the modes ν_{8a}, ν_{7a}, and ν_{19a}. The frequencies of the last two are higher when the *ortho* substituent is a methoxy group ($[FeL^{dimet}]^{+\cdot}$, $[FeL^{o\text{-}met}]^{+\cdot}$) compared with *tert*-butyl-substituted phenoxyl ($^3[L^{p\text{-}met}]^{+\cdot}$) (see Table 6). This tendency may be due to an increase in the C=O double bond character in the *ortho*-methoxy substituted species. The C–O bond length calculated for the free *ortho*-methoxy phenoxyl radical (*o*-CH_3O-PhO$^\cdot$) is 1.250 Å, which is shorter by ≈0.007 Å than the corresponding bond lengths of the *para*-substituted or unsubstituted phenoxyl radicals. Consequently, a substantial increase in the calculated frequencies is observed for the modes ν_{7a} and ν_{19a}.

Furthermore, a methoxy substituent in the *ortho* position leads to an elongation of the adjacent C_{ortho}–C_{meta} bond (1.393 Å) compared with the *para*-methoxy phenoxyl radical (*p*-CH_3O-PhO$^\cdot$; 1.379 Å). Hence, the frequency of the corresponding stretching mode ν_{8a} is calculated at 1575 cm^{-1}, which is 20 cm^{-1} lower than for *p*-CH_3O-PhO$^\cdot$.[8] This tendency is also observed for the coordinated radicals inasmuch as the mode ν_{8a} of $[FeL^{o\text{-}met}]^{+\cdot}$ is ≈20 cm^{-1} lower than in complexes that include a *para*-methoxy-substituted phenoxyl radical. The frequency shift of ν_{8a} reduces the energy separation with respect to the mode ν_{7a}, particularly since the latter mode undergoes a slight increase in energy. These frequency changes are paralleled by an increase in the relative RR intensity of ν_{7a} with respect to ν_{8a}, which has also been observed for di-*tert*-butylphenoxyl complexes[8] and can be rationalized in terms of the normal composition of the mode ν_{7a}. An increase in frequency indicates a larger contribution of the C=C stretching coordinate, which is expected to exhibit the most pronounced changes upon $\pi \rightarrow \pi^*$ excitation and, therefore, provides the strongest contribution to the RR intensity. Conversely, an increase in the C=C stretching character of mode ν_{7a} leads to an increase in the C–O stretching contribution to the adjacent ν_{19a} mode. Hence, the observed frequency shifts and intensity changes of mode ν_{7a} merely reflect a redistribution of the normal mode composition. This conclusion has significant impact for extracting structural information from the RR spectra of phenoxyl-radical complexes inasmuch as mode ν_{7a} does not constitute a sensitive marker for the C–O bond strength, and, indirectly, for the strength of the metal–radical interactions.

One might have expected that the metal–oxygen stretch is a more appropriate marker. However, attempts to identify this mode in the low-frequency region based on $^{18}O/^{16}O$ shifts failed. Presumably, the resonance enhancement for this mode is relatively low at excitation in resonance with the $\pi \rightarrow \pi^*$ transition. In addition, in previous studies on $[ML^{p\text{-}met}]$ radical complexes with different metal ions we found that the bands between 650 and 500 cm^{-1} reveal only minor variations with the nature of the metal ion.[8] Thus, it may be that for the coordinated phenoxyl ligand the metal–oxygen stretching coordinate is distributed among several modes so that the expected metal-sensitivity (and the $^{18}O/^{16}O$ substitution) is reflected only by small changes in the frequencies of several modes.

For $[FeL^{dimet}]^{+\cdot}$ the visible absorption band is broadened and the maximum shifts from ≈520 to 610 nm compared with the reduced complex (Figure 2). This finding indicates that the Fe–phenoxyl CT transition contributes to this absorption band and/or the Fe–phenolate CT transitions are affected upon formation of a coordinated phenoxyl radical. Excitation lines between 510 and 600 nm yield RR spectra that display exclusively bands of the two phenolate rings, whereas no bands attributable to the coordinated phenoxyl can be identified (Figure 7). The resonance enhancement for the

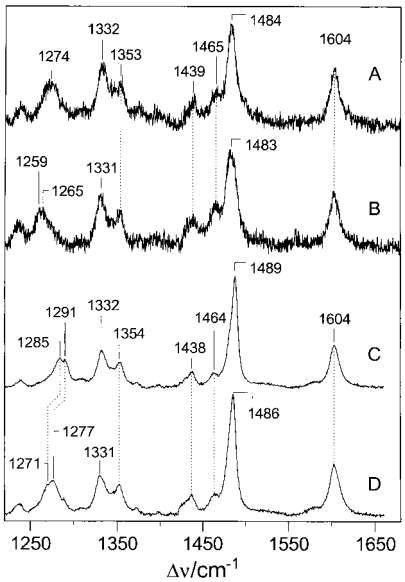

Figure 7. RR spectra of (**A**) $[FeL^{dimet}]^{+\cdot}$ and (**B**) the ^{18}O-labeled $[FeL^{dimet}]^{+\cdot}$, (**C**) $[FeL^{dimet}]$, and (**D**) the ^{18}O-labeled $[FeL^{dimet}]$. The excitation wavelengths were 598 (**A**, **B**) and 514 nm (**C**, **D**). The Raman bands of the solvent (CH_2Cl_2/tBu_4NPF_6) are subtracted.

phenoxyl modes is relatively weak upon excitation in resonance with the CT transition.[8] This observation is in line with results obtained for a mono(phenolato)iron radical complex that does not include additional coordinated phenolates. RR spectra of this species excited in resonance with the CT transition show only a few bands of extraordinarily weak intensity.[41] Thus, it is not surprising that the RR spectra of $[FeL^{dimet}]^{+\cdot}$ and $[FeL^{dimet}]$ obtained by excitation with visible light are very similar and that the subtle spectral differences reflect the effect of oxidation of one aromatic ring on the ground-state structure of the two remaining phenolates. In particular, we note shifts of the modes that include the C–O stretching coordinate. The mode ν_{19a} shifts down from 1489 cm^{-1} by 5 cm^{-1}, whereas an even larger decrease (−11 cm^{-1}) is observed for the ν_{7a} modes, which in $[FeL^{dimet}]^{+\cdot}$ overlap to give a broad peak centered at about 1275 cm^{-1}.

0947-6539/99/0509-2562 $ 17.50+.50/0 *Chem. Eur. J.* **1999**, *5*, No. 9

There appears to be a qualitative correlation between the magnitude of these shifts and the contribution of the C–O stretching coordinate involved in these modes as indicated by the $^{18}O/^{16}O$-isotopic shifts. Thus, it is concluded that radical formation is associated with a weakening of the C–O bond of the coordinated phenolates obviously due to a net electron-density transfer from the phenolates to the electron-deficient phenoxyl. Such a charge redistribution should lead to a strengthening of the $Fe–O_{phenolate}$ bond, which, in turn, should be reflected by an increase in the frequency of the Fe–O stretching modes. In fact, the bands of [FeL^{dimet}] at 615 and 573 cm^{-1} attributable to modes including the Fe–O stretching are shifted up by 1 and 5 cm^{-1}, respectively, in the RR spectrum of the radical complex [FeL^{dimet}]$^{+\bullet}$.

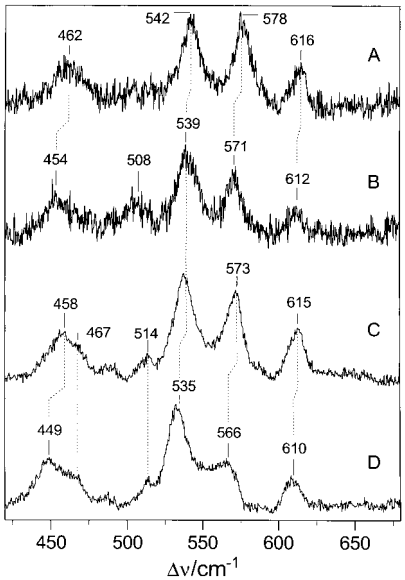

Figure 8. RR spectra of (**A**) [FeL^{dimet}]$^{+\bullet}$ and (**B**) the ^{18}O-labeled [FeL^{dimet}]$^{+\bullet}$, (**C**) [FeL^{dimet}], and (**D**) the ^{18}O-labeled [FeL^{dimet}]. The excitation wavelengths were 598 (**A**, **B**) and 514 nm (**C**, **D**). The Raman bands of the solvent (CH_2Cl_2/$t$$Bu_4NPF_6$) are subtracted.

Experimental Section

Synthesis: Preparations of the ligands H_3L^{but}, $H_3L^{p\text{-}met}$, and complexes [FeL^{but}], [$FeL^{p\text{-}met}$] were carried out as described previously.[3]

2,4-Dimethoxyphenol was selectively labeled with ^{18}O at the phenol oxygen by the following procedure. An argon-flushed solution of 1-bromo-2,4-dimethoxybenzene (1.0 g, 4.6 mmol) and isopropyl bromide (0.85 g, 6.9 mmol) in dry tetrahydrofuran (THF) was added to magnesium turnings (0.28 g, 11.52 mmol) in a Schlenk flask under an argon atmosphere. The solution was stirred rapidly at 20 °C until formation of the Grignard reagent began, after which point the vessel was cooled in a cold-water bath. After 2 h of stirring at 20 °C the Grignard reagents were transferred to a Schlenk flask (500 mL) containing degassed dry pentane (100 mL). The cooled mixture (−126 °C) was allowed to react with $^{18}O_2$ whilst it was slowly warmed to 20 °C. This mixture was then stirred for 20 h and the resulting precipitate was collected by filtration. The cream-gray residue was added to dilute aqueous HCl (50 mL) and extracted with CH_2Cl_2 (2 × 50 mL). The combined organic phases were dried over Na_2SO_4 and the solvent removed on a rotary evaporator. Column chromatography of the resulting oil (CH_2Cl_2, G60 SiO_2 gel) gave two products: 1,3-dimethoxybenzene and 2,4-dimethoxy phenol. The phenol moved down the column as a pale yellow band. Combination of the fractions containing pure phenol and removal of the solvent gave a total yield of 0.27 g of phenol. GC-MS (product mixture): m/z (%): 156 ([M]$^+$, 100), 154 (21), 155 (3), 157 (7). This implies about 83% incorporation of ^{18}O at the phenolic oxygen position.

1,4,7-Tris(3,5-dimethoxy-2-hydroxybenzyl)-1,4,7-triazacyclononane (H_3L^{dimet}): A mixture of paraformaldehyde (22.5 mg, 0.75 mmol) in methanol (3 mL) was added to a solution of 1,4,7-triazacyclononane (32.3 mg, 0.25 mmol) in dry methanol (2 mL). The mixture was refluxed under a flow of argon for 2 h before 2,4-dimethoxyphenol (127 mg, 0.82 mmol) dissolved in CH_3OH (4 mL) was added. The resulting solution was refluxed for 4 h and stirred at 20 °C for 5 days. After removal of the solvent by a rotary evaporation a sticky, brown gum of H_3L^{dimet} was obtained and used for synthesis of the complexes without further purification or characterization.

[$Fe^{III}L^{dimet}$]: The above ligand mixture was redissolved in CH_3OH (5 mL), and $FeCl_3$ (40.5 mg, 0.25 mmol) in CH_3OH (5 mL) was then added with stirring. Addition of triethylamine (1.5 mL) caused a dramatic color change from deep blue to deep purple. After stirring for 3 h at 20 °C, the solution was filtered and the precipitate washed with CH_3OH (1 mL) and recrystallized from acetonitrile. Red-purple crystals of [$Fe^{III}L^{dimet}$]·2CH_3CN were obtained in 42% yield. $C_{37}H_{48}N_5O_6Fe$: calcd C 58.27, H 6.34, N 9.16; found C 58.2, H 6.22, N 9.0. ESI MS: m/z (%): 681 ([M + H]$^+$, 100). The ^{18}O-labeled complex was prepared analogously (ESI MS: m/z (%): 687 ([M + H]$^+$, 100)). From the isotopic pattern and comparison with unlabeled material it followed that species containing 3, 2, and 1 ^{18}O labels are present in approximately 57, 33, and 7%, respectively.

1,4,7-Tris(3-methoxy-5-*tert*-butyl-2-hydroxybenzyl)-1,4,7-triazacyclononane ($H_3L^{o\text{-}met}$): This ligand was prepared as described above for H_3L^{dimet} from 2-methoxy-4-*tert*-butylphenol[3] as starting material. The crude ligand was not isolated or characterized but used directly for complex formation.

[$FeL^{o\text{-}met}$]: The complex was prepared as described above for [FeL^{dimet}]. The crude product was recrystallized from a CH_2Cl_2/CH_3CN mixture (1:1). Deep purple-red microcrystals of [$Fe^{III}L^{o\text{-}met}$] were obtained. $C_{42}H_{60}N_3O_6Fe$: calcd C 66.48, H 7.97, N 5.54; found C 66.34, H 8.02, N 5.46. ESI MS: m/z (%): 759 ([M + H]$^+$, 20), 781 ([M + Na]$^+$, 100), 797 ([M + K]$^+$, 15).

EPR and Mössbauer spectroscopy: For the EPR measurements a Bruker ESP 300E continuous wave X-band spectrometer with a Bruker dual-mode cavity and a helium-flow cryostat (Oxford Instruments ESR 910) was used. The field was calibrated with a Bruker NMR gaussmeter and the frequency was measured with a HP frequency counter. Mössbauer data were recorded on alternating constant-acceleration spectrometers with minimum experimental line-width 0.24 mm s^{-1} (full-width at half-height). The sample temperature was maintained in either an Oxford Instruments Variox or an Oxford Instruments Mössbauer-Spectromag cryostat. The latter is a split-pair, superconducting magnet system for applied fields of up to 8 T where the temperature of the sample can be varied over the range 1.5–250 K. The field at the sample is oriented perpendicular to the γ-beam. The $^{57}Co/Rh$ source (1.8 GBq) was positioned at room temperature inside the gap of the magnet system at a zero-field position. Isomer shifts are quoted relative to iron metal at 300 K.

Magnetic Mössbauer spectra were analyzed on the basis of a spin Hamiltonian description of the electronic ground state spin multiplet [Eq. (4)], where $S_t = 5/2$, 2, or 3/2 is the spin of the corresponding system (see

$$H_e = D[S_{t,z}^2 - S_t(S_t+1)/3 + (E/D)_t(S_{t,x}^2 - S_{t,y}^2)] + \mu_B \mathbf{B}\cdot g\cdot \mathbf{S}_t \quad (4)$$

text), and D_t and E/D_t are the axial and rhombic zero-field parameters with respect to S_t. For the simulation of the hyperfine interaction we have taken into account the Hamiltonian [Eq. (5)], where $\langle \mathbf{S}_t \rangle$ is the electronic spin expectation value, A_t is the hyperfine coupling tensor, $\mathbf{I}$ is the nuclear spin, and H_Q is the usual nuclear quadrupole Hamiltonian.[42]

$$H_{hf} = \langle \mathbf{S}_t \rangle A_t \mathbf{I} - g_N \mu_N \mathbf{B}\mathbf{I} + H_Q \quad (5)$$

Resonance Raman spectroscopy: RR spectra were recorded with a U 1000 spectrograph (2400/mm holographic gratings) equipped with a liquid-nitrogen-cooled CCD detector (Instruments SA). The output of a dye laser (Coherent 899-01), an argon ion laser (Coherent Innova 400), and a krypton ion laser (Coherent Innova 302) served as excitation sources. The laser power at the sample was about 50 mW. In order to avoid photo-induced degradation, the sample, which exhibits an optical density of about

1.5 at the excitation wavelength, was deposited in a rotating cell. The Raman scattered light was detected in 90° with a scrambler placed in front of the entrance slit of the spectrometer to account for the polarization sensitivity of the gratings. The spectral slit width was 2.8 cm^{-1}. The spectra, measured with an acquisition time of 50 s, were linearized in wavenumbers yielding an increment between 0.1 and 0.25 cm^{-1} and a total spectral range of 500 cm^{-1}. The contributions of the solvent and the supporting electrolyte were subtracted.

Quantum chemical calculations: All quantum chemical computations were performed by means of the Gaussian 92/DFT suite of ab initio programs working under OpenVMS and were carried out on a DEC station 2000 as described in detail elsewhere.[8] For density functional theory (DFT) computations we employed the Becke3LYP (B3LYP) combination of hybrid exchange and correlation functions.[43] For all neutral phenoxyl radicals, the 6-31G* basis sets were applied.[44] These basis sets are of double zeta type for the valence electrons and they are augmented by d-polarization functions for the carbon and oxygen atoms. For the phenolate the 9s5p/4s2p basis set augmented with polarization functions was employed. Moreover, for oxygen and carbon additional diffuse s- and p-functions are provided with exponents of 0.059 and 0.034, respectively.[45] The frequencies were scaled by a factor of 0.9744 as discussed previously.[8]

X-ray crystallography: A suitable single crystal ($0.45 \times 0.11 \times 0.11$ mm) of $[Fe^{III}L^{dimet}] \cdot 2CH_3CN$ was mounted on a glass fiber on a Siemens SMART diffractometer. Measurements were performed with graphite-monochromated $Mo_{K\alpha}$ radiation ($\lambda = 0.71073$ Å). Intensities were corrected for absorption effects with the SADABS program (G. M. Sheldrick, **1994**). The structure was solved by direct methods with SHELXTL. Non-hydrogen atoms were refined with anisotropic thermal parameters; hydrogen atoms were included with isotropic thermal parameters. One acetonitrile solvent molecule was disordered. The disorder was satisfactorily modeled by two positions with occupancy factors of 0.5 for two terminal atoms treated as carbon (C(41), C(41X)). Crystallographic data are given in Table 7.

Table 7. Crystallographic data for $[Fe^{III}L^{dimet}] \cdot 2MeCN$.

chem formula	$C_{37}H_{48}FeN_5O_9$
fw	762.65
space group	$P2_1/n$
a [Å]	12.373(2)
b [Å]	26.448(5)
c [Å]	12.398(2)
β [°]	116.00(2)
V [Å^3]	3646.5(11)
Z	4
T [K]	100(2)
ρ calcd [g cm^{-3}]	1.389
$\mu(Mo_{K\alpha})$ [cm^{-1}]	4.76
refl. collected	31587
unique refl./$[I > 2\sigma(I)]$	7604 / 5518
no. parameters	477
$2\theta_{max}$ [°]	55.0
$R1$[a] $[I > 2\theta(I)]$	0.0642
$wR2$[b] $[I > 2\theta(I)]$	0.1296

[a] $R1 = \Sigma ||F_o| - |F_c|| / \Sigma |F_o|$. [b] $wR2 = [\Sigma[w(F_o^2 - F_c^2)^2] / \Sigma[w(F_o^2)^2]]^{1/2}$, where $w = 1/\sigma^2(F_o^2) + (aP)^2 + bP$, $P = (F_o^2 + 2F_c^2)/3$.

Crystallographic data (excluding structure factors) have been deposited with the Cambridge Crystallographic Data Centre as supplementary publication no. CCDC-102115. Copies of the data can be obtained free of charge on application to CCDC, 12 Union Road, Cambridge CB2 1EZ, UK (fax: (+44) 1223-336-033; e-mail: deposit@ccdc.cam.ac.uk).

Acknowledgments

The authors thank the Fond der Chemischen Industrie for financial support. P.H. acknowledges a Heisenberg fellowship from the Deutsche Forschungsgemeinschaft.

[1] J. Hockertz, S. Steenken, K. Wieghardt, P. Hildebrandt, *J. Am. Chem. Soc.* **1993**, *115*, 11222.
[2] A. Sokolowski, E. Bothe, E. Bill, T. Weyhermüller, K. Wieghardt, *Chem. Commun.* **1996**, 1671.
[3] B. Adam, E. Bill, E. Bothe, B. Goerdt, G. Haselhorst, K. Hildenbrand, A. Sokolowski, S. Steenken, T. Weyhermüller, K. Wieghardt, *Chem. Eur. J.* **1997**, *3*, 308.
[4] A. Sokolowski, J. Müller, T. Weyhermüller, R. Schnepf, P. Hildebrandt, K. Hildenbrand, E. Bothe, K. Wieghardt, *J. Am. Chem. Soc.* **1997**, *119*, 8889.
[5] A. Sokolowski, B. Adam, T. Weyhermüller, A. Kikuchi, K. Hildenbrand, R. Schnepf, P. Hildebrandt, E. Bill, K. Wieghardt, *Inorg. Chem.* **1997**, *36*, 3702.
[6] A. Sokolowski, H. Leutbecher, T. Weyhermüller, R. Schnepf, E. Bothe, E. Bill, P. Hildebrandt, K. Wieghardt, *J. Biol. Inorg. Chem.* **1997**, *2*, 444.
[7] J. Müller, T. Weyhermüller, E. Bill, P. Hildebrandt, L. Ould-Moussa, T. Glaser, K. Wieghardt, *Angew. Chem.* **1998**, *110*, 637; *Angew. Chem. Int. Ed.* **1998**, *37*, 616.
[8] R. Schnepf, A. Sokolowski, J. Müller, V. Bachler, K. Wieghardt, P. Hildebrandt, *J. Am. Chem. Soc.* **1998**, *120*, 2352.
[9] a) M. M. Whittaker, J. W. Whittaker, *J. Biol. Chem.* **1988**, *263*, 6074; b) M. M. Whittaker, V. D. DeVito, S. A. Asher, J. W. Whittaker, *J. Biol. Chem.* **1989**, *264*, 7104; c) M. L. McGlashen, D. D. Eads, T. G. Spiro, J. W. Whittaker, *J. Phys. Chem.* **1995**, *99*, 4918; d) K. Clark, J. E. Penner-Hahn, M. M. Whittaker, J. W. Whittaker, *J. Am. Chem. Soc.* **1990**, *112*, 6433.
[10] M. M. Whittaker, P. J. Kersten, N. Nakamura, J. Sanders-Loehr, E. S. Schweizer, J. W. Whittaker, *J. Biol. Chem.* **1996**, *271*, 681.
[11] a) U. Auerbach, U. Eckert, K. Wieghardt, B. Nuber, J. Weiss, *Inorg. Chem.* **1990**, *29*, 938; b) U. Auerbach, T. Weyhermüller, K. Wieghardt, B. Nuber, E. Bill, C. Butzlaff, A. X. Trautwein, *Inorg. Chem.* **1993**, *32*, 508.
[12] P. G. Debrunner in *Mössbauer Spectroscopy of Iron Porphyrins, Vol. III* (Ed.: P. G. Debrunner), VCH, Weinheim, **1989**, pp. 137–234.
[13] U. Russo, G. J. Long, in *Mössbauer Spectroscopic Studies of the High Oxidation States of Iron, Vol. 3* (Eds.: U. Russo, G. J. Long), Plenum, New York, London, **1989**, pp. 289–329.
[14] D. Mandon, R. Weiss, K. Jayaraj, A. Gold, J. Terner, E. Bill, A. X. Trautwein, *Inorg. Chem.* **1992**, *31*, 4404–4409.
[15] L. Shu, J. C. Nesheim, K. Kauffmann, E. Münck, J. D. Lipscomb, L. Que, *Science* **1997**, *275*, 515.
[16] T. Jüstel, T. Weyhermüller, K. Wieghardt, E. Bill, M. Lengen, A. X. Trautwein, P. Hildebrandt, *Angew. Chem.* **1995**, *107*, 744; *Angew. Chem. Int. Ed. Engl.* **1995**, *34*, 669.
[17] T. Jüstel, M. Müller, T. Weyhermüller, C. Kressl, E. Bill, P. Hildebrandt, M. Lengen, M. Grodzicki, A. X. Trautwein, B. Nuber, K. Wieghardt, *Chem. Eur. J.* **1999**, *5*, 793–810.
[18] U. Knof, T. Weyhermüller, K. Wieghardt, E. Bill, C. Butzlaff, A. X. Trautwein, *Angew. Chem.* **1993**, *105*, 1701; *Angew. Chem. Int. Ed. Engl.* **1993**, *32*, 1635.
[19] K. L. Kostka, B. G. Fox, M. P. Hendrich, T. J. Collins, C. E. F. Rickard, L. J. Wright, E. Münck, *J. Am. Chem. Soc.* **1993**, *115*, 6746.
[20] T. J. Collins, K. L. Kosta, E. Münck, E. S. Uffelmann, *J. Am. Chem. Soc.* **1990**, *112*, 5637.
[21] T. J. Collins, B. G. Fox, Z. G. Hu, K. L. Kosta, E. Münck, C. E. F. Rickard, L. J. Wright, *J. Am. Chem. Soc.* **1992**, *114*, 8724.
[22] D. Sellmann, S. Emig, F. W. Heinemann, *Angew. Chem.* **1997**, *109*, 1808; *Angew. Chem. Int. Ed. Engl.* **1997**, *36*, 1734.
[23] D. Sellmann, S. Emig, F. W. Heinemann, F. Knoch, *Angew. Chem.* **1997**, *109*, 1250; *Angew. Chem. Int. Ed. Engl.* **1997**, *36*, 1201.
[24] P. Gütlich, R. Link, A. Trautwein, *Mössbauer Spectroscopy and Transition Metal Chemistry*, Springer, Berlin, Heidelberg, New York, **1978**.
[25] E. Münck, in *Iron-Sulfur Proteins*, *Vol. 3* (Ed.: T. G. Spiro), Wiley, New York, **1982**, p. 147.
[26] For the concentrated solution (1.5 mM) the spectra showed an additional broad absorption-derivative signal at $g \approx 2$ that changed upon dilution. However, the pattern persisted even at 20 μM concentration and varied for different preparations. We suppose that the neutral complexes tend to aggregate in solution. The resulting enhanced intermolecular spin-spin interaction could give rise to the

  0947-6539/99/0509-2564 $ 17.50+.50/0

collapsed signal at $g \approx 2$. On the other hand, such a feature could not be reasonably well simulated with the usual rhombic spin Hamiltonian [Eq. (4)].
[27] N. N. Greenwood, T. C. Gibb, *Mössbauer Spectroscopy*, Chapman and Hall, London, **1971**.
[28] The described magnetic anisotropy of the ground-state Kramers doublet is obtained in the calculations with $E/D_t \approx 1/3$, $D_t > 0$. For $E/D = 1/3$, however, the sign of D is without physical meaning, since the highest Kramers doublet has equivalent magnetic properties, except that y and z axes are virtually interchanged. This means that the internal field would be oriented along the z direction instead of the y direction. Hence, the same Mössbauer simulation would be obtained with $D_t < 0$ and $V_{x'x'}$ oriented in the z direction.
[29] The large asymmetry parameter was essentially confirmed by the symmetric hyperfine pattern of a magnetically perturbed measurement (7 T) at 160 K, which indicated that η is close to 1. However, under these conditions spin relaxation appeared to be in an intermediate range with respect to the nuclear precession rate as the spectrum was not satisfactorily resolved. We therefore refrain from depicting the result of a preliminary simulation, performed with the Hamiltonian [Eqs. (4),(5)] in the limit of fast or slow relaxation.
[30] P. Gütlich, in *Mössbauer Spectroscopy*, *Vol. 5* (Ed.: U. Gonser), Springer, Berlin, Heidelberg, **1975**, p. 53.
[31] E. Simanek, Z. Sroubek, in *Electron Paramagnetic Resonance* (Ed.: S. Geschwind), Plenum, New York, London, **1972**, p. 535.
[32] A similar effect is discussed for 3s electrons that can be polarized by negative spin density in the overlap region of metal–ligand bonds, see ref. [31].
[33] J. T. Sage, Y.-M. Xia, P. G. Debrunner, D. T. Keough, J. D. Jersey, B. Zerner, *J. Am. Chem. Soc.* **1989**, *111*, 7239–7247.
[34] J. H. Rodriguez, H. Ok, Y.-M. Xia, P. G. Debrunner, B. E. Hinrichs, T. Meyer, N. H. Packard, *J. Phys. Chem.* **1996**, *100*, 6849–6862.
[35] A. Mukherjee, M. L. McGlashen, T. G. Spiro, *J. Phys. Chem.* **1995**, *109*, 4912- 4917.
[36] I. Harada, H. Takeuchi in *Spectroscopy of Biological Systems* (Eds.: R. J. H. Clark, R. E. Hester), Wiley, New York, **1986**, pp. 113–175.
[37] O. Nwobi, J. Higgins, X. Zhou,R. Liu, *Chem. Phys. Lett.* **1997**, *272*, 155–161.
[38] L. Öhrström, I. Michaud-Soret, *J. Am. Chem. Soc.* **1996**, *118*, 3283–3284.
[39] J. W. Pyrz, A. L. Roe, L. J. Stern, L. Que, Jr., *J. Am. Chem. Soc.* **1985**, *107*, 614–620.
[40] C. J. Carrano, M. W. Carrano, K. Sharma, G. Backes, J. Sanders-Loehr, *Inorg. Chem.* **1990**, *29*, 1865–1870.
[41] J. Müller, L. Ould-Moussa, P. Hildebrandt, unpublished results.
[42] A. X. Trautwein, E. Bill, E. L. Bominaar, H. Winkler, *Struct. Bonding (Berlin)* **1991**, *78*, 1.
[43] a) A. D. Becke, *J. Chem. Phys.* **1993**, *98*, 5648–5652; b) G. Lee, W. Young, R. G. Parr, *Phys. Rev.* **1988**, *B37*, 785–789; c) B. Miehlich, A. Savin, H. Stoll, H. Preuss, *Chem. Phys. Lett.* **1989**, *157*, 200–206.
[44] a) W. J. Hehre, R. Ditchfield, J. A. Pople, *J. Chem. Phys.* **1972**, *56*, 2257–2261; b) P. C. Hariharan, J. A. Pople, *Theor. Chim. Acta* **1973**, *28*, 213–222; c) M. S. Gordon, *Chem. Phys. Lett.* **1980**, *76*, 163–168; d) T. Clark, J. Chandrasekhar, G. W. Spitznagel, P. von R. Schleyer, *J. Comp. Chem.* **1983**, *4*, 294–301.
[45] T. H. Dunning, P. J. Hay, *Modern Theoretical Chemistry*, Plenum, New York, **1976**.

Received: December 2, 1998 [F1472]